INVESTIGATION OF THE DENSITY STRUCTURE
OF THE THIN WATER-AIR BOUNDARY LAYER

E. P. Anisimova, A. A. Pivovarov, A. A. Speranskaya,
and V. P. Sukhanov

Findings of an experimental investigation of the heat transfer mechanism at work
in the thin water-air boundary layer in the absence of advective transport are
presented. Data are cited on values of the coefficient of turbulent heat trans-
fer in the thin surface layer of air over the water and in the near-surface layer
of the water, estimates are offered for the ratio of the coefficients of turbu-
lent thermal diffusivity and turbulent diffusion of moisture, and the Bowen num-
ber is calculated.

One of the important modes of interaction between water reservoirs and the atmosphere
is heat transfer between the surface of the water and adjacent air layers. The heat trans-
fer rate is governed by processes at work in the very tenuous boundary layers on either
side of the water-air interface. Investigation of the structure of these near-surface
layers under natural conditions runs into aggravating difficulties. Study of the mechanism
underlying heat transfer in the thin water-air boundary layer in the absence of advective
transport is facilitated by the laboratory experiment we set up.

The experimental arrangement comprised a thick-walled heat-insulated glass vessel of
cylindrical shape, 28 cm in diameter and standing 35 cm high [1]. A frame of thin Plexi-
glas was placed inside the vessel, and temperature sensors were mounted on that frame.
The vessel was filled with water at room temperature. A massive heater unit with a built-
in watertight electrical helix winding was mounted at the top in such a manner that the
bottom surface of the heater came into contact with the water. The temperature field in
the water and in the thin layer of air near the water surface was investigated using copper-
constantan thermocouples with o.26 mm diameter thermal junctions. The temperature reading
was taken relative to the temperature at the bottom of the vessel, where the cold junctions
of the thermocouples and a control resistance thermometer were positioned. The temperature
was determined to within ±0.1° by means of a PP-63 potentiometer. Use of a N-115 loop
oscillograph to record data made it possible to record temperature fluctuations over a fre-
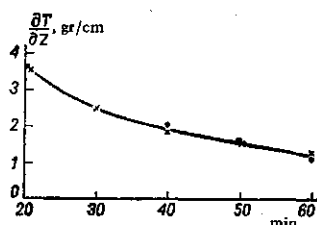quency range of 0 to 1 Hz in air.

Fig. 1. Comparison of calculated
and instrumentally measured temper-
ature gradients in air; dots indi-
cate calculated values and crosses
indicate empirically measured values.

Temperature profiles near the water-air
interface were measured using 21 sensors.
These were mounted on a common rod and were
spaced 2 mm apart. The sensors were electri-
cally switched onto recorder. The rod carry-
ing the sensors could be immersed totally
into the water or could be withdrawn and set
vertically or at a 45° angle to the surface
of the water. A post carrying the thermo-
couples was free to move along the vessel
diameter. Preliminary experiments were
staged during the project in order to study
the temperature field throughout the interior
and over the surface of the vessel, and these findings showed that the downward-propogating
heat flux levels out rapidly horizontally, remaining uneven only near the walls. Isolines
of the temperature in the water run parallel to each other, attesting to propogation of heat

solely in the vertical direction. All of the measurements described below were carried out in the middle portion of the vessel, and were started after the heater had been removed and the water surface had reached the temperature pf 45°C.
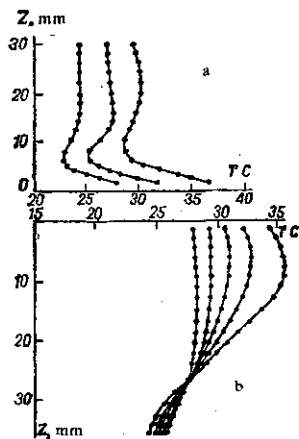

Fig. 2. Two series of measured temperature profiles: a) in air; b) in water. Time (reading left to right): a) 50, 20, 5; b) 30, 25, 15, 10.

The temperature profiles were measured in water and in air by the method of sequentially interrogating the sensors. It took 4 min to complete one profile. The temperature profiles were then referred to a single instant of time for subsequent analysis. Plots of the time variation of temperature provided information on the cooling rate of air and water $\partial T/\partial \tau$ for each layer. Vertical temperature gradients $\partial T/\partial z$ were calculated from the temperature profiles referred to a single instant of time. The vertical temperature gradient was also determined by instrumental means, using a differential battery consisting of six copper-constantan thermocouples [2]. The sensor baseline during the measurements was 2 mm. Values of the measured gradients averaged over 3-min time spans can be compared to profiles of the mean temperature for the layer of air near the water surface as plotted in Fig. 1. The difference between the measured and predicted values is not greater than 5%.

Detailed temperature profiles resulted from the experiment conducted in the tenuous layer of air near the water surface (30 mm) and in the surface layer of water adjacent to the water-air interface (40 mm). The time variability of the temperature of water and air was also successfully traced on each layer of measurements and in terms of the profiles as a whole. Some series of examples of temperature profiles in air and in water are shown in Fig. 2. The numerals referred to particular profiles denote the time, in minutes, elapsed from the start of the experiment. The equipment used made it possible to measure the temperature in air starting 2 mm from the interface, while a sensor corresponding to the z = 0 level was placed directly beneath the water surface, so as to measure the mean temperature in the 0-0.5 mm layer. The temperature of the water-air interface was not ascertained by the authors. The temperature of the water near the surface is lower than in the underlying layers on all of the profiles so obtained—in other words what is termed a cold film was observed on the surface of the water.

Estimates of the heat transfer coefficient in water as a function of depth K(z) were obtained from the resulting experimental data. The experimental conditions allowed us to ignore volume sources of heat and to resort to the one-dimensional heat conduction equation in the form

$$\frac{\partial T}{\partial \tau} = \frac{1}{\rho^2} \frac{\partial}{\partial z} \left[\rho^2 k(z) \frac{\partial T}{\partial z} \right]. \tag{1}$$

Neglecting the temperature dependence of the water density $\rho = \rho(T)$, which is due to slight temperature drops in the layer under investigation (maximum temperature drop not exceeding 3°C), and integrating Eq. (1) from 0 to z, we obtain

$$K(z) = \frac{-\int_0^z \frac{\partial T}{\partial \tau} \, dz + K(0) \frac{\partial T}{\partial z}\Big|_{z=0}}{\frac{\partial T}{\partial z}\Big|_{z=z}}. \tag{2}$$

It has been shown in numerous investigations [3-6] that molecular heat transfer plays a decisive role near the surface in a thin layer of water on the order of 1 mm. In this case K(0) in Eq. (2) can be put equal to the coefficient of molecular thermal diffusivity.

Using the empirically obtained $\partial T/\partial \tau$ and $\partial T/\partial z$ and calculating the integral $\int_0^z \frac{\partial T}{\partial \tau} \, dz$ by the trapezoidal rule, we then find K(z). Results of calculations using Eq. (2) are plotted in Fig. 3 for comparison with data reported by other authors and obtained on the basis of measurements performed at sea [7,8], on a river [9], and in a lake [10]. The results of all these calculations can be approximated by the formula

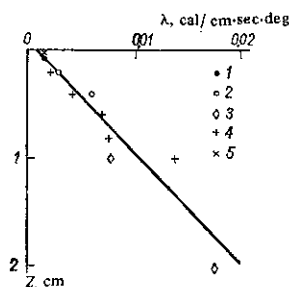$$\lambda = \lambda_m + az, \tag{3}$$

14

Fig. 3   Fig. 4

Fig. 3. Change in thermal diffusivity in the thin surface layer of water: 1) according to [7]; 2) according to [9]; 3) according to [10]; 5) according to [8]; 4) data reported in the present article.
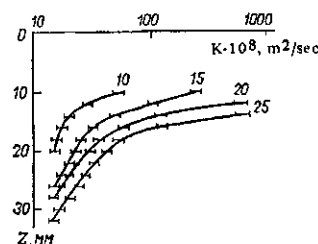
Fig. 4. Results of thermal diffusivity calculations for below the temperature discontinuity layer.

where λ_m is the molecular thermal diffusivity coefficient, a is a proportionality factor whose numerical value is $1.05 \cdot 10^{-2}$ cal/(sec·cm²·deg). Accordingly, the value of $\partial\lambda/\partial z$ can be taken as constant within the limits of a layer such as described. This means that the data from a laboratory experiment carried out under conditions where there is no advective heat transport agree with data obtained in full-scale investigations with low wind forces and low wave forces present.

When $z = 1$ cm, the predicted λ value (Fig. 3) will be higher than the value derived from the linear relationship (3). This is probably because developed convective motion is already present on this layer. Figure 2b confirms that supposition: within 15 min after cooling is started an isothermal interval expanding with the time shows up on the temperature profile. The upper bound of the interval attains $z = 4$ mm within 20 min and then remains constant within the limits of accuracy of our measurements, while the lower bound gradually drops to reach 30 mm within 30 min. A layer exhibiting a negative temperature gradient (temperature discontinuity layer) lies below the isothermy layer. This discontinuity layer plays the role of a "liquid" bottom (artificial bottom) and acts as hindrance to convection advancing toward the near-bottom layers of the water where the temperature remains virtually constant throughout the experiment.

The presence of this constant temperature stands in the way of our using Eq. (2) to calculate $K(z)$ below the $z = 1$ cm level. We can resort to the following means to estimate the intensity of thermal processes at work below the layer engaged in developed convective flow. As mentioned earlier, heating of the water surface sets in when temperature equilibrium prevails throughout the bulk phase of the water, so that all of the thermal processes are determined by molecular characteristics. The temperature rose in response to this heating only at the top of the vessel, and the temperature in the lower-lying layers remained unchanged throughout the experiment. Now if we put $K(z_1) = K_{mol}$ at point z_1 with constant temperature, we can use Eq. (2) by simply changing the integration limits. The results of these calculations are plotted in Fig. 4. The $K(z)$ values below the temperature discontinuity layer are not much greater than the molecular values (by a factor of 5 to 6 at most), and an increase in $K(z)$ by several tenfold is noted in the transition across the discontinuity layer.

Consequently, for the temperature drop (water—air) $\approx 20°C$ we investigated, some time after the onset of cooling in the water we observe developed convective flow at a certain depth. A boundary layer characterized by a positive temperature gradient and maintaining a stable existence forms in the immediate vicinity of the surface, despite the unstable density stratification in the layer. The thickness of this boundary layer is ≈ 4 mm in the case in point. At distances from the surface commensurate with the boundary layer thickness, we cannot afford to neglect molecular thermal conduction. The range of convection heat transfer is bounded below by the temperature discontinuity layer. The thermal diffusivity falls off rapidly in the transition through this layer, and below the layer it assumes values close to those of the molecular coefficients.

Temperature profiles in the thin layer of air overlying the water, are shown in Fig. 2a, for the case of a water surface in the process of colling off. All of the measured

temperature profiles are characterized by appreciable temperature gradients (up to 470 deg/m) near the surface. Moreover, starting with some layer the temperature gradient reverses sign, i.e., a layer of inverted temperature distribution shows up.

The turbulent heat transfer in air can be found as a function of height on the basis of the experimental data. The shape of the empirically measured temperature profiles allows us to neglect bulk sources of heat on layers below the inversion layer, and enables us to make use of Eq. (1). We cannot afford to neglect the temperature dependence of density throughout the layer under investigation in this instance, for the reason that, unlike the water, the entire volume of air under study was divided into 2 mm thick horizontal layers. The assumption was that density varies stepwise on the boundaries of the layers, while $\rho = const$ within the confines of each layer. In that case Eq. (1) becomes simplified, and by integrating Eq. (1) from level z_1 to level z_2, we arrive at a formula for $K(z)$ in the form

$$ K(z_2) = \frac{\int_{z_1}^{z_2} \frac{\partial T}{\partial \tau}\, dz + K(z_1)\, \frac{\partial T}{\partial z}\Big|_{z=z_1}}{\frac{\partial T}{\partial z}\Big|_{z=z_2}}. \qquad (4) $$

The value of K has to be known on each of the horizons, in order to perform calculations using Eq. (4). Using arguments similar to those marshalled in the discussion of calculations based on Eq. (2), we can put K equal to the molecular thermal diffusivity of air at the temperature of the water surface on the horizon $z = 0$. Then Eq. (4) will allow us to find, given the experimentally derived $\partial T/\partial \tau$ and $\partial T/\partial z$ values, the value of K for each temperature profile. Results of these calculations are entered in Table 1.

Table 1

5 min after start of cooling			20 min after start of cooling		
z, mm	T °C	K, 10^2 cm²/sec	z, mm	T °C	K, 10^2 cm²/sec
2	35,8	65	2	31,1	48
4	32,4	76	4	27,1	58
6	29,4	128	6	25,1	260
8	28,5	450			

It is clear from Table 1 that the turbulent thermal diffusivities are only slightly in excess of the molecular diffusivities at the temperatures in question.

Traces of temperature pulsations taken in air at the 1 mm, 3 mm, and 5 mm layers (from the surface of the water) show (note examples displayed in Fig. 5) that turbulent temperature pulsations are observed in the thin layer of air near the water surface.

Measurements of mean moisture and of pulsations of relative moisture $r(z)$ were taken at various horizons in the layer of air near the water surface, in addition to temperature measurements. The relative humidity was recorded using a specially engineered hygrograph [11] which featured a hair 4 cm long positioned horizontally as sensor, and a mechanically controlled vacuum tube, the type 6MKh2B mechanotron, recording slight elongations of that hair. The time constant of the hydrograph was 0.45 sec. The profiles of temperature and relative humidity were employed in computing the specific humidity $q(z)$ at various layers, and the air density profile (see example in Fig. 5) was calculated from the equation of state of moist air. It is clear from Fig. 5 that the density distribution varies monotonically with height, and that stratification of density throughout the thickness of air investigated is unstable.

We realize from Fig. 5 that the relative humidity attains values of 96-98% in the immediate vicinity of the water surface ($z \leq 3$ mm). This means that close to water vapor saturation can be assumed in the thin layer of air near the water surface (~3 mm). That statement is strikingly confirmed by records taken of humidity pulsations on precisely those horizons. The behavior of the humidity pulsations alters abruptly as we get closer to the surface. The pulsations become more asymmetrical and, moreover, the humidity spikes are directed only in the direction of decrease, while pulsations of both signs show up at higher horizons (at humidities on the order of 80%).

These profiles were plotted on a semilogarithmic scale (Fig. 6) in order to ascertain the shape of the dependences T(z) and q(z) in the layer of air adjacent to the water
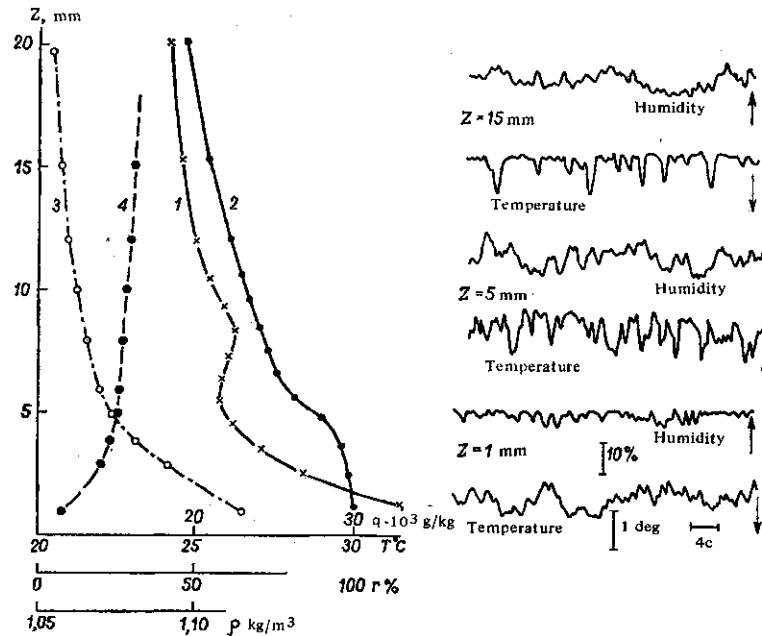
16

Fig. 5. Examples of profiles of mean temperatures (1), of relative humidity (2), specific humidity (3), and of air density (4), and records of pulsations in temperature and relative humidity at various horizons above the water surface.
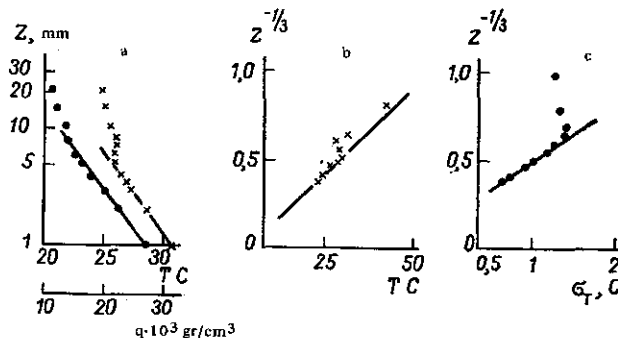

Fig. 6. Height distribution of the mean and rms temperatures in different intervals of the thin surface layer of air adjacent to the water surface.

surface. It is evident in Fig. 6 that the temperature profile below the inversion layer obeys the logarithmic law closely. As for the specific humidity, it is distributed logarithmically in height up to 2 mm, i.e., up to the termination of the inversion layer. Accordingly, the shape of the temperature profile and specific humidity profile in the layer of air adjacent to the water surface allows us to make use of the theory of a logarithmic boundary layer. And clearly, in that case we can resort to the formula [12]:

$$\frac{T_*}{q_*} = \frac{K_T}{K_E} \frac{\partial T/\partial z}{\partial q/\partial z},$$ (5)

where T_* and q_* are the temperature scale and humidity scale, K_T is the turbulent thermal diffusivity, K_E is the eddy diffusivity of the moisture, and $\partial q/\partial z$ is the specific humidity gradient.

Once the ratio T_*/q_* is determined, we can find from Eq. (5) the ratio of the turbu-

17

lent thermal diffusivity and turbulent moisture diffusion. In order to find T_*/q_*, we make use of the fact that the temperature and humidity profiles near the water surface obey a logarithmic law, so that the values of T_* and q_* can be readily found from the slope of the temperature and humidity profiles on a semilogarithmic scale. The ratio T_*/q_* turned out to be $5 \cdot 10^2$. Then, computing the gradients appearing in Eq. (5) on the basis of the experimental data, we can estimate the ratio K_T/K_E. The results of these calculations appear in Table 2.

Table 2

z, mm	T °C	q, g/kg	K_T/K_E	B_0
1	30,5	26,0	0,96	0,195
2	28,6	22,5	0,90	0,206
3	26,9	20,2	1,15	0,211
4	26,2	17,6	1,50	0,204
5	25,7	15,9	—	0,195
6	25,8	14,85	—	0,175
8	26,0	13,65	—	0,168

It is clear from the tabular data that the ratio K_T/K_E is close to unity all the way up to the temperature inversion layer. This means that the temperature profiles and specific humidity profiles are similar, and that the heat transfer and moisture diffusion mechanisms at work in this layer are identical.

The Bowen number, by definition equal to the ratio of heat flux and moisture flow, is an important dimensionless characteristic of the layer of air adjacent to the water surface. Its significance lies in its value for estimating the contribution made by moisture to density stratification. Upon calculating the ratio T_*/q_*, we can estimate the Bowen number, since we have

$$B_0 = \frac{c_p}{L} \frac{T_*}{q_*}. \tag{6}$$

With that formulation, we get $B_0 = 0.207$. The estimate so obtained is in close agreement with B_0 values calculated on the basis of measurements taken above the sea surface [12]. The Bowen number can also be determined from data on temperature and humidity profile measurements [13]:

$$B_0 = \frac{c_p (T_0 - T_a)}{L (q_0 - q_a)}. \tag{7}$$

Note that Eq. (7) for the Bowen number is valid only provided we have $K_T/K_E = 1$. Results of calculating the number B_0 using Eq. (7) are listed in Table 2. Results of calculations based on Eq. (6) and Eq. (7) agree in the layer directly adjacent to the water surface, which once again serves to confirm that the transfer coefficient ratio in that layer is unity.

Analysis of the measurements data reveals that the temperature profile above the inversion layer closely obeys the Prandtl-Obukhov free convection law [11] (see Fig. 6b):

$$T(z) = f(z^{-1/3}).$$

Root-mean-square values of the temperature fluctuations at those heights are also proportional to $z^{-1/3}$ (Fig. 6c), i.e., Priestley's dependence [14] obtained for free convection is satisfied at those heights. Analysis of traces of temperature pulsations showed that the nature of these temperature pulsations above the inversion layer contrasts markedly with the shape of the pulsations below the inversion layer. Starting at height 5 mm, discrete spurts of more than a degree show up against a background of random temperature pulsations, and on horizons above the inversion layer the temperature pulsations exhibit the form typical of convection flow: short-duration spikes in the direction of increasing temperature and more protracted states characterized by the almost complete absence of oscillations.

Accordingly, analysis of the experimental data reveals that the layer of air adjacent to the water surface can be separated into two distinct zones, in the absence of advective transport and when there is intense chilling of the water surface. At the top of the layer of air adjacent to the water surface ($z \geq 8$ mm, i.e., above the temperature inversion layer) we find free convection prevailing. Evidence of this is provided by the shape of the temperature profiles and rms values of temperature pulsations, and also by the appearance of records of the temperature pulsations at those heights. In the immediate neighborhood of the water surface, the temperature and humidity obey a logarithmic law of distribution with height (with $z = 1$ mm taken as the lower horizon in the measurements). The boundary between zones is fuzzy, and encompass a certain layer within which the temperature field becomes restructured and where a temperature inversion is observed on the averaged profiles. Elements of both convective motion and thermal turbulent boundary layer are present here.

REFERENCES

1. V. P. Sukhanov, in collection: Comprehensive Research in the World Ocean [in Russian], Moscow, 1975.
2. E. P. Anisimova and A. A. Speranskaya, Vestnik Mosk. Univ. Fizika, Astron., no. 6, 1964.
3. E. G. Andreev, V. S. Lavorko, A. A. Pivovarov, and G. G. Khundzhua, Okeanologiya, vol. 9, no. 2, 1969.
4. F. K. Ball, Austr. J. Physics, vol. 7, pp. 649-652, 1954.
5. H. U. Roll, Deutsche Hydrogr. Zs., vol. 5, pp. 141-143, 1952.
6. E. D. McAlister, W. McLeish, and E. A. Corduen, J. Geophysic. Res., vol. 76, no. 18, 1971.
7. E. D. McAlister and W. McLeish, J. Geophys. Res., vol. 74, pp. 3408-3414, 1969.
8. E. G. Andreev, V. V. Gurov, and G. G. Khundzhua, Proceedings of the 5th All-Union Conference on Heat Transfer and Mass Transfer [in Russian], Kiev, vol. 10, 1976.
9. V. K. Al'tberg and E. A. Popov, Izv. GGI [State Hydrological Inst.], no. 67, 1934.
10. M. P. Timofeev and S. P. Malevskii-Malevich, Meteorologiya i Gidrologiya, no. 2, 1967.
11. E. P. Anisimova, A. A. Speranskaya, and V. P. Sukhanov, The Hair Hygrograph, in collection: Informational Materials on Hydrometeorological Instruments and Observational Techniques; Collection of Articles No. 63 [in Russian], Moscow, 1975.
12. A. S. Monin and A. M. Yaglom, Statistical Fluid Mechanics, part 1 [in Russian], Moscow, 1965.
13. S. A. Kitaigorodskii, Physics of Atmosphere-Ocean Interaction [in Russian], Leningrad, 1970.
14. R. S. Bortkovskii, E. K. Byutner, L. Yu. Preobrazhenskii, and S. P. Malevskii-Malevich, Transport Processes Near the Ocean-Atmosphere Interface [in Russian], Leningrad, 1974.
15. H. B. Priestley, Turbulent Transport in the Ground Layer of the Atmosphere [Russian translation] Leningrad, 1964.

11 September 1976

Department of Physics of the Sea
and of Landlocked Water Bodies